

Adaptive Variational Model for Contrast Enhancement of Low-Light Images*

Po-Wen Hsieh[†], Pei-Chiang Shao[‡], and Suh-Yuh Yang[§]

Abstract. Contrast enhancement plays an important role in image/video processing and computer vision applications. Its main purpose is to adjust the image intensity to enhance the quality and features of the image. In this paper, we propose a simple and efficient adaptive variational model for contrast enhancement for partially shaded low-light images. The key idea of this adaptive approach is to employ the maximum image of the RGB color channels as a classifier to divide the image domain into the relatively bright and dim parts, and then use different fitting terms for each part such that the bright pixels are preserved as close as possible to the original ones while the dim pixels are boosted with brightness and contrast-level parameters to adjust the degree of the strength. With this adaptivity, one can find that the proposed model considerably improves upon the existing variational models in the literature. In this paper, the existence and uniqueness of the minimizer for the variational minimization problem is established. The split Bregman method is used to accomplish an efficient numerical implementation of the adaptive variational model. Moreover, a number of numerical experiments and comparisons with other popular enhancement methods are conducted to demonstrate the high performance of the newly proposed method.

Key words. contrast enhancement, image enhancement, adaptive variational model, nonuniform illumination, low-light images

AMS subject classifications. 68U10, 65K10

DOI. 10.1137/19M1245499

1. Introduction. As is well known, nonuniform illumination during the image acquisition process, e.g., shadows, night time scenes, and other inadequate lighting conditions, highly affects the dynamic range of captured digital images and usually results in images with very low contrast regions. Low contrast not only leads to unpleasing or unclear images for human vision but can also further lead to poor detection or understanding for machine vision. As a result, contrast enhancement is a fundamental and very important step for most of the tasks in image/video processing and computer vision applications. The main goal of contrast enhancement is to improve image quality by making hidden image details and features clearer

*Received by the editors February 19, 2019; accepted for publication (in revised form) October 14, 2019; published electronically January 7, 2020.

<https://doi.org/10.1137/19M1245499>

Funding: This work was supported by the Ministry of Science and Technology of Taiwan under grants MOST 106-2115-M-005-005-MY2, MOST 107-2811-M-008-007, MOST 106-2115-M-008-014-MY2, and MOST 108-2115-M-008-012-MY3. The work of the third author was partially supported by the National Center for Theoretical Sciences, Taiwan.

[†]Department of Applied Mathematics, National Chung Hsing University, South District, Taichung City 40227, Taiwan (pwhsieh@nchu.edu.tw).

[‡]Department of Mathematics, Soochow University, Shihlin District, Taipei City 11102, Taiwan (shaopj823@gmail.com).

[§]Department of Mathematics, National Central University, Jhongli District, Taoyuan City 32001, Taiwan (syyang@math.ncu.edu.tw, <http://www.math.ncu.edu.tw/~syyang/>).

and more discernible for better human visual perception or machine vision identification. In recent years, contrast enhancement has been widely used for many types of low-contrast images in various fields, such as medical images (CT, MRI, X-ray, ultrasound, etc.), remote-sensing images (ecology, geology, military, planning, etc.), electron microscopy images (biological, chemical, material, etc.), and even everyday photography.

In the past few decades, many contrast enhancement methods have been developed, and they can be classified into categories according to the taxonomy used. For example, enhancement methods can be broadly classified into direct methods [6, 16] and indirect methods [41, 47], depending on whether there exists a contrast measure [24] defined in the model. However, most popular methods are in the second category, which can be further divided into three groups [39]: spectral methods, histogram methods, and spatial methods. First, spectral methods, also called transform-domain methods, mainly rely on Fourier or wavelet transforms. The input image is first decomposed into several subbands or scales, and then the enhancement is performed by applying some nonlinear operators to the transform coefficients in the appropriate subbands or scales [28].

Second, histogram methods use predefined transfer functions to adjust the image histogram by stretching or redistributing pixel values in the intensity range of the processed image. The most representative and widely used histogram method is the so-called histogram equalization (HE) [26, 27, 51]. Because of its simplicity and satisfactory performance, HE becomes the most commonly used method for contrast enhancement. Using the cumulative distribution function of the intensity of input pixels as the transform function, HE achieves a uniform distributed histogram, which implies maximum transfer of information [14, 17]. According to the way the image histogram is modified, histogram methods can further be categorized into two types: global methods and local methods [1, 3, 25]. Generally speaking, global methods use the histogram information of the entire input image to do the transformation, which is often insufficient to achieve good contrast enhancement since it fails to adapt with the intensity changes of local image features. On the other hand, in order to adapt the global methods to small-scale details, local histogram methods are proposed [12, 13, 40, 48, 50], which modify image intensities using a local histogram obtained from pixels in a prescribed small window. The local adaptivity is usually much better at improving the contrast. However, the computational cost for local methods is also high, and overenhancement and artifacts are sometimes presented in the processed image.

Methods in the third group are the spatial methods, where image intensities are directly modified to enhance the image according to some spatial constraints or hypothesis about the human visual system. In [9], Boccignone and Picariello exploited a nonlinear scale-space representation of the anisotropic diffusion of Perona–Malik type [36] in a multiscale framework. In a series of works by Gatta, Rizzi, and Marini [21, 45, 46], they proposed and studied an effective method, called automatic color equalization (ACE), based on modeling the mechanism of the human visual system such that the enhancement process is consistent with human perception. Later, Bertalmío et al. [8] linked the previous ACE approach with variational techniques so that the properties and behavior of the ACE can be studied via the associated energy functional. Furthermore, Getreuer [22] gave fast approximation and implementation of the ACE method. On the other hand, in a series of works by Caselles, Provenzi, and their coauthors [7, 35, 42], they proposed a perceptually inspired variational framework for color

image enhancement and studied its relation with the retinex theory [29, 43]. In [39], Pierre et al. employed the average local contrast measure to enhance images and approximately preserve the hue for color images within a variational framework.

In the recent work of Morel, Petro, and Sbert [34], they proposed a simple variational model, composed of a data fidelity term and a regularization term, to alleviate the effect caused by nonuniform illumination and preserve image details at the same time. More specifically, their model can be written as

$$(1.1) \quad \min_u \frac{1}{2} \int_{\Omega} |\nabla u - \nabla f|^2 d\mathbf{x} + \frac{\lambda}{2} \int_{\Omega} (u - \bar{u})^2 d\mathbf{x},$$

where Ω represents the image domain, ∇ the gradient operator, f the input image, u the desired image, and $\bar{u} := \frac{1}{|\Omega|} \int_{\Omega} u d\mathbf{x}$ the mean value of u over Ω . The first term in the variational minimization problem (1.1) acts as the data fidelity term, forcing u to preserve the image gradient, while the second term acts as the regularization term, reducing the variance of u to eliminate the effect of nonuniform illumination. In addition, $\lambda > 0$ is a constant parameter which balances between detail preservation and variance reduction. Generally speaking, if λ tends to zero, then the desired image u coincides with the original image f . Conversely, if λ is sufficiently large, then the desired image u approaches the constant \bar{u} . In [34], the authors also showed that when λ gets large the model acts as a high-pass filter (edge detector). Interested readers are referred to Figure 11 in [34] for the enhanced results with $\lambda = 0.0001, 0.0005, 0.001$, and 0.005 . Later, the data term is then modified in [38] and applied in [4] using the L^1 norm instead of the L^2 norm to deal with discontinuities and obtain sharper edges. Although reasonable numerical results for nonuniform medical images and hazy images have been obtained in [4, 34, 38], there is still plenty of room for improvement.

In this paper, we will revisit the variational model (1.1) for contrast enhancement of low-light images. In fact, we will propose a novel adaptive variational model. The key idea of the proposed model is to employ the maximum image of the RGB color channels as a classifier to divide the image domain into the relatively bright and dim parts, and then use different fitting terms for each part such that the bright pixels are preserved as close as possible to the original ones while the dim pixels are boosted with brightness and contrast-level parameters to adjust the degree of the strength. With this adaptivity, one can find that the newly proposed model significantly improves the existing variational models in the literature. In this paper, the existence and uniqueness of the minimizer for the variational minimization problem will be established. The split Bregman method will be used to accomplish an efficient numerical implementation of the adaptive variational model. In addition, numerical comparisons with some other popular enhancement methods will be provided.

The remainder of this paper is organized as follows. In section 2, we introduce the adaptive contrast enhancement model and give the mathematical analysis on the existence and uniqueness of the minimizer. In section 3, we show that the adaptive variational model can be solved efficiently using the split Bregman iterative scheme. Numerical experiments are conducted in section 4 to demonstrate the high performance of the newly proposed model. Finally, some concluding remarks are given in section 5.

2. The adaptive variational model. In this section, we first propose an adaptive variational model for the enhancement of grayscale images; this is then generalized to the enhance-

ment of RGB color images. We can find that the regularization parameter and the brightness and contrast-level parameters of the model are intuitive and easy to tune. Also, the unique solvability of the variational minimization problem will be theoretically guaranteed in this section.

2.1. Enhancement of grayscale images. Given a low-contrast input image f , the goal of contrast enhancement is to find a desired image u whose gradient is close to that of f but with reduced variance to balance inhomogeneous illumination. Extended from model (1.1), let us first consider the following variational model for image contrast enhancement:

$$(2.1) \quad \min_u \frac{1}{q} \int_{\Omega} |\nabla u - \nabla f|^q d\mathbf{x} + \frac{\lambda}{2} \int_{\Omega} (u - \bar{u})^2 d\mathbf{x},$$

where $q = 1$ or 2 . As is well known in variational image processing, ∇u , ∇f , and $\nabla u - \nabla f$ are all sparse in most situations, and $q = 1$ ensures more sparsity than $q = 2$. Generally speaking, an enhanced image obtained from (2.1) with $q = 2$ will be much smoother, and one obtained from (2.1) with $q = 1$ will tend to preserve image structures. From another viewpoint, $q = 2$ comes from the assumption that $\nabla u - \nabla f$ is Gaussian distributed, while $q = 1$ comes from the assumption that $\nabla u - \nabla f$ is Laplacian distributed. As is experimented in [31], $\nabla u - \nabla f$ matches Laplacian distribution better than Gaussian distribution. Consequently, it is generally more reasonable to use $q = 1$ in model (2.1) than $q = 2$.

Since the Euler–Lagrange equation of model (2.1) is highly nonlinear and difficult to solve, [34] linearizes it (for the case $q = 2$) by assuming that the mean value of u coincides with the mean value of f . Therefore, the following variational minimization problem can be considered instead:

$$(2.2) \quad \min_u \frac{1}{q} \int_{\Omega} |\nabla u - \nabla f|^q d\mathbf{x} + \frac{\lambda}{2} \int_{\Omega} (u - \bar{f})^2 d\mathbf{x},$$

where the mean value of f over Ω , $\bar{f} := \frac{1}{|\Omega|} \int_{\Omega} f d\mathbf{x}$, replaces the \bar{u} used in model (2.1). This model is much simpler and more computationally tractable. Numerical results showing acceptable performance can be found in [4, 34, 38].

Despite its simplicity and effectiveness, model (2.2) still has room for improvement. First, requiring the desired image u to be close to a pixel-independent \bar{f} seems unreasonable, which highly contradicts the requirement of ∇u being close to ∇f and restrains parameter λ to being very small. Second, the lack of contrast-level parameters to adjust the strength of enhancement makes model (2.2) less flexible.

With enhancing low-light images as the goal, we propose two adaptive (pixel-dependent) functions g and h to replace the pixel-independent constant \bar{f} and the original input image f in (2.2), respectively. The model reads as

$$(2.3) \quad \min_u \frac{1}{q} \int_{\Omega} |\nabla u - \nabla h|^q d\mathbf{x} + \frac{\lambda}{2} \int_{\Omega} (u - g)^2 d\mathbf{x} + \chi_S(u),$$

where the adaptive functions g , h and the characteristic function χ_S with $S := [0, 255]$ (cf. Remark 2.3 below) are defined respectively as follows:

$$(2.4) \quad g(\mathbf{x}) := \begin{cases} \alpha \bar{f}, & \mathbf{x} \in \Omega_d := \{\mathbf{x} \in \Omega : f(\mathbf{x}) \leq \bar{f}\}, \\ f(\mathbf{x}), & \mathbf{x} \in \Omega_b := \{\mathbf{x} \in \Omega : f(\mathbf{x}) > \bar{f}\}, \end{cases}$$

with a brightness parameter $\alpha > 0$,

$$(2.5) \quad h(\mathbf{x}) := \begin{cases} \beta f(\mathbf{x}), & \mathbf{x} \in \Omega_d := \{\mathbf{x} \in \Omega : f(\mathbf{x}) \leq \bar{f}\}, \\ f(\mathbf{x}), & \mathbf{x} \in \Omega_b := \{\mathbf{x} \in \Omega : f(\mathbf{x}) > \bar{f}\}, \end{cases}$$

a contrast-level parameter $\beta > 1$, and

$$(2.6) \quad \chi_S(u) := \begin{cases} 0, & \text{range}(u) \subseteq S, \\ +\infty & \text{otherwise.} \end{cases}$$

We call Ω_d the dim part and Ω_b the bright part of the image domain Ω . It is worth pointing out that the second term in the newly proposed model (2.3) acts not only as a regularization term but partially as a data fidelity term as well, since the adaptive function g in (2.4) is defined as the original image value $f(\mathbf{x})$ for \mathbf{x} in the bright part Ω_b .

To complete this subsection, we further give the following three remarks on g , h , and χ_S , which explain the motivation derived behind the adaptive enhancement model (2.3).

Remark 2.1. For nonuniformly illuminated low-light image f , we divide the image domain Ω into dim part Ω_d and bright part Ω_b such that $\Omega = \Omega_d \cup \Omega_b$ and $\Omega_d \cap \Omega_b = \emptyset$, using \bar{f} , the mean intensity of f , as the division baseline. For $\mathbf{x} \in \Omega_d$, dim elements are supposed to be boosted by requiring the desired image u to be close to $\alpha \bar{f}$, where larger α makes hidden image details and features clearer and more discernible, and the contrast-level parameter β is employed to enhance the local gradient in the dim area Ω_d . For $\mathbf{x} \in \Omega_b$, bright elements are supposed to be retained by requiring the desired image u to be close to their already visible level $f(\mathbf{x})$.

Remark 2.2. To ensure the differentiability of h in (2.3), in practice we smooth the coefficients in (2.5) and redefine the adaptive function h as

$$(2.7) \quad h(\mathbf{x}) = G * (\beta 1_{\Omega_d}(\mathbf{x}) + 1_{\Omega_b}(\mathbf{x})) f(\mathbf{x}), \quad \mathbf{x} \in \Omega,$$

where the indicator function $1_A(\mathbf{x}) = 1$ if $\mathbf{x} \in A$, otherwise $1_A(\mathbf{x}) = 0$, and $G*$ represents suitable Gaussian convolution such that ∇h is well-defined.

Remark 2.3. The characteristic function $\chi_S(u)$ is zero if the intensity values of u are all within the closed bounded interval S and $+\infty$ outside. Adding $\chi_S(u)$ to the energy functional is equivalent to constraining the minimization of the energy functional over some suitable function space with image range being equal to S . In practice, two reasonable choices of S are $[\inf f(\mathbf{x}), \sup f(\mathbf{x})]$ and $[0, 255]$. For simplicity, we take $S = [0, 255]$ throughout this paper.

2.2. Enhancement of color images. The enhancement model (2.3) with the adaptive functions g and h is designed for grayscale low-light images. Now, we need to generalize the previous domain-division procedure for a color image, with which we can then process RGB color images channelwise. By bright part, we mean pixels defined in Ω that are already clearly visible (e.g., the sky and the river in Figure 1(a)), while by dim part, we mean pixels that are low-lighted and ambiguously invisible (e.g., the house and the pathway in Figure 1(a)). The goal is to classify pixels in Ω into these two groups and enhance the dim one. There may be

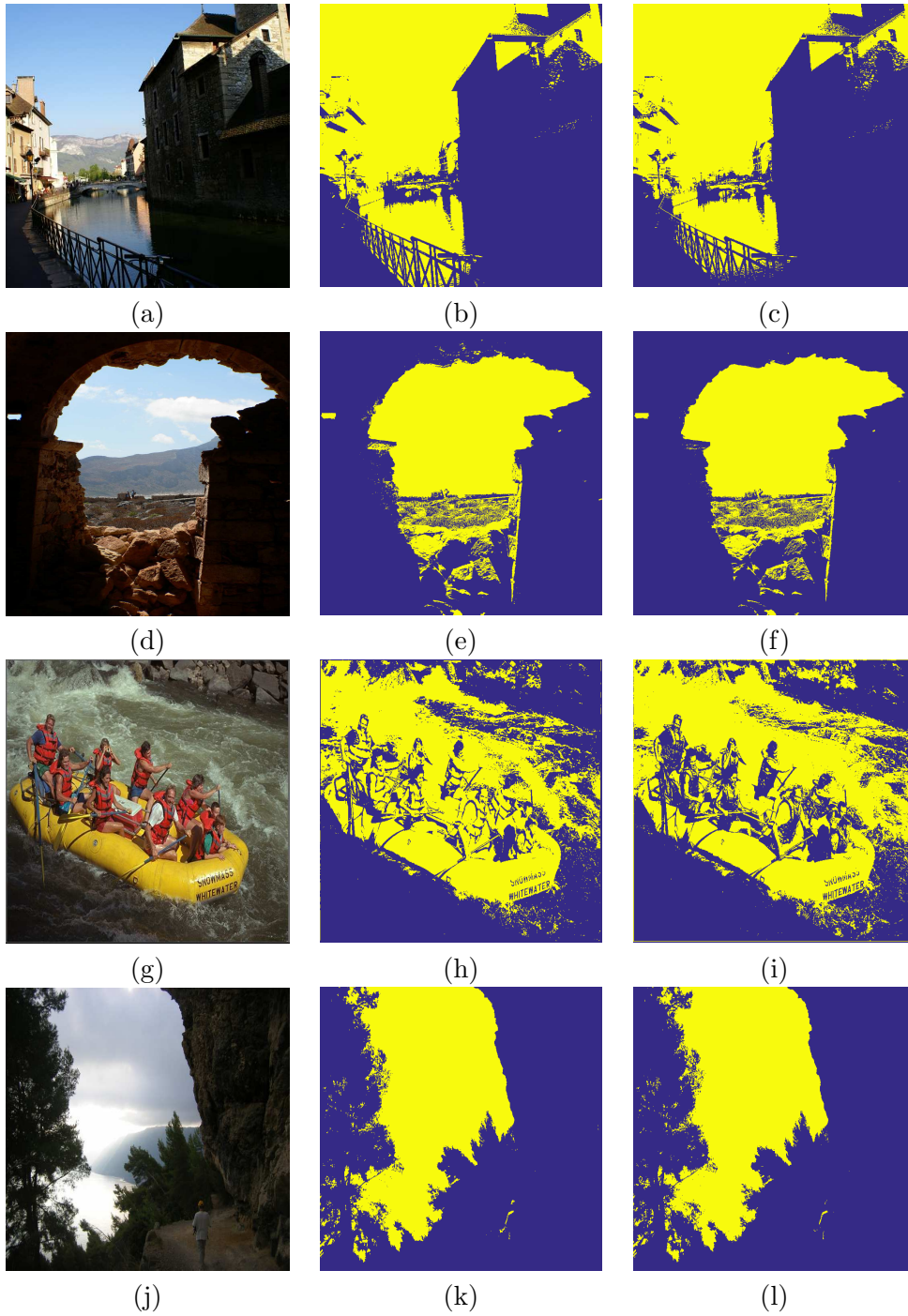


Figure 1. Several low-light images and the corresponding domain divisions: (a), (d), (g), and (j) are test images used in Example 4.3 below; (b), (e), (h), and (k) are the results of domain division by the proposed maximum image $\max\{f_R, f_G, f_B\}$; (c), (f), (i), and (l) are the results of domain division by the grayscale image $0.299f_R + 0.587f_G + 0.114f_B$.

many possible ways to achieve this goal; any one that leads to a reasonable domain division is acceptable.

Here we propose a simple way to address the domain-division problem. Denoting by (f_R, f_G, f_B) the given color image to be enhanced, we first define the maximum image as

$$(2.8) \quad f_{\max}(\mathbf{x}) := \max\{f_R(\mathbf{x}), f_G(\mathbf{x}), f_B(\mathbf{x})\},$$

where the max operator is performed pointwisely on each $\mathbf{x} \in \Omega$. Let $\bar{f}_{\max} := \frac{1}{|\Omega|} \int_{\Omega} f_{\max} d\mathbf{x}$. Then we divide the image domain Ω into two parts,

$$(2.9) \quad \Omega_d := \{\mathbf{x} \in \Omega : f_{\max}(\mathbf{x}) \leq \bar{f}_{\max}\},$$

$$(2.10) \quad \Omega_b := \{\mathbf{x} \in \Omega : f_{\max}(\mathbf{x}) > \bar{f}_{\max}\}.$$

The domain-division results of several low-light images given in Figures 1(a), 1(d), 1(g), and 1(j) using (2.9)–(2.10) are depicted in Figures 1(b), 1(e), 1(h), and 1(k), respectively. Regions of Ω_d and Ω_b are presented visually by blue and yellow, respectively. The division results are apparently acceptable, and the blue regions (Ω_d) need to be enhanced.

We find empirically that using the maximum image as the classifier will give reasonable divisions. This result is not surprising since the maximum image is proportional to the value channel of the HSV representation, where $V := \max\{f_R, f_G, f_B\}/255 = f_{\max}/255$. Therefore, f_{\max} and V will give the same correct division result. However, other classifiers may lead to erroneous division. For example, Figures 1(c), 1(f), 1(i), and 1(l) are the division results using the grayscale image $f_{\text{gray}} := 0.299f_R + 0.587f_G + 0.114f_B$ as classifier. One can find that there are some pixels misclassified by f_{gray} . Specifically, in Figure 1(c), the river around the bike is classified into dim parts, and in Figure 1(i), the life jackets, which are visually clear, are also misclassified into dim parts.

Another possibility is to perform domain division channelwise. However, this approach will result in a hue-preservation problem. As an example, consider an element $\mathbf{x}^* \in \Omega$ with color intensities $(f_R(\mathbf{x}^*), f_G(\mathbf{x}^*), f_B(\mathbf{x}^*)) = (10, 10, 200)$; then $f_{\max}(\mathbf{x}^*) = f_B(\mathbf{x}^*) = 200$, a large value. Employing f_{\max} (or equivalently the V channel) as classifier, \mathbf{x}^* will be classified into Ω_b as a bright element, as desired. As a result, $(f_R(\mathbf{x}^*), f_G(\mathbf{x}^*), f_B(\mathbf{x}^*))$ will be preserved as close as possible to $(10, 10, 200)$ by the model, and the hue will be preserved at \mathbf{x}^* . However, if we perform the domain division channelwise, then pixel \mathbf{x}^* will be classified into Ω_d in the R and G channels and be classified into Ω_b in the B channel. As a result, $f_B(\mathbf{x}^*)$ will be preserved as close as possible to 200, while $f_R(\mathbf{x}^*)$ and $f_G(\mathbf{x}^*)$ will be enhanced to, say, 60. Therefore, the hue will not be preserved at \mathbf{x}^* , leading to unnatural images. In view of this, we do not consider channelwise domain division in this paper.

With the help of the maximum image f_{\max} , we can now process color images channelwise. For every $f \in \{f_R, f_G, f_B\}$, we solve

$$(2.11) \quad \min_u \frac{1}{q} \int_{\Omega} |\nabla u - \nabla h_c|^q d\mathbf{x} + \frac{\lambda}{2} \int_{\Omega} (u - g_c)^2 d\mathbf{x} + \chi_S(u),$$

where the adaptive functions g_c and h_c are defined by

$$(2.12) \quad g_c(\mathbf{x}) := \begin{cases} \alpha \bar{f}, & \mathbf{x} \in \Omega_d, \\ f(\mathbf{x}), & \mathbf{x} \in \Omega_b, \end{cases}$$

$$(2.13) \quad h_c(\mathbf{x}) := \begin{cases} \beta f(\mathbf{x}), & \mathbf{x} \in \Omega_d, \\ f(\mathbf{x}), & \mathbf{x} \in \Omega_b, \end{cases}$$

with Ω_d and Ω_b defined in (2.9) and (2.10), respectively.

We complete this subsection by remarking that the regularization parameter λ , the brightness parameter α , and the contrast-level parameter β are all fixed across channels. At this stage, there is no evidence shown that choosing different λ , α , and β for each channel separately has a specific benefit. Therefore, we fix λ , α , and β across channels in this paper.

2.3. Mathematical analysis. In this subsection, we will prove the existence and uniqueness of the minimizers of the variational minimization problems (2.3) and (2.11) in some suitable function space. We first discuss the case $q = 1$ for model (2.3). To begin with, we present some basic results for the bounded variation space $BV(\Omega)$ as below, and more details can be found in, e.g., [2, 10].

Definition 2.4. Let Ω be an open subset of \mathbb{R}^2 . The space of functions of bounded variation $BV(\Omega)$ is defined as the space of real-valued function $u \in L^1(\Omega)$ such that the total variation

$$\int_{\Omega} |Du| := \sup \left\{ \int_{\Omega} u \operatorname{div} \varphi \, d\mathbf{x} : \varphi \in C_c^1(\Omega, \mathbb{R}^2), \|\varphi\|_{L^\infty(\Omega)} \leq 1 \right\}$$

is finite. Then $BV(\Omega)$ is a Banach space with the norm

$$\|u\|_{BV(\Omega)} := \|u\|_{L^1(\Omega)} + \int_{\Omega} |Du|.$$

The next two lemmas characterize the sequential compactness and lower semicontinuity properties of the bounded variation space $BV(\Omega)$ (cf. Theorem 3.23 and Proposition 3.6 in [2] or Theorems 2.1.2 and 2.1.1 in [10], respectively).

Lemma 2.5. Suppose sequence $\{u_n\} \subset BV(\Omega)$ satisfies $\sup \|u_n\|_{BV(\Omega)} < \infty$. Then there exist a subsequence $\{u_{n_k}\}$ and a function $u \in BV(\Omega)$ such that

$$u_{n_k} \rightarrow u \text{ in } L^1(\Omega) \text{ as } k \rightarrow \infty.$$

Lemma 2.6. Assume $\{u_n\} \subset BV(\Omega)$ and $u_n \rightarrow u$ in $L^1(\Omega)$. Then

$$\int_{\Omega} |Du| \leq \liminf_{n \rightarrow \infty} \int_{\Omega} |Du_n|.$$

Now we are in a position to prove the existence and uniqueness of the minimizer of (2.3) with $q = 1$, and then the same assertion holds for (2.11) immediately. The suitable solution space for the variational minimization problem (2.3) should be $BV(\Omega) \cap L^2(\Omega)$.

Theorem 2.7. Let $\Omega \subset \mathbb{R}^2$ be an open bounded domain with smooth C^2 boundary, and let h defined in (2.7) be in the space $W^{1,2}(\Omega)$. Then the variational minimization problem (2.3) with $q = 1$ admits a unique minimizer in $\Lambda := \{u \in BV(\Omega) \cap L^2(\Omega) : 0 \leq u(\mathbf{x}) \leq 255 \text{ a.e. in } \Omega\}$.

Proof. We will consider the variational minimization problem (2.3) with $q = 1$ over the function space $BV(\Omega) \cap L^2(\Omega)$. Introducing the new variable $w := u - h \in BV(\Omega) \cap L^2(\Omega)$, then problem (2.3) with $q = 1$ can be written as

$$(2.14) \quad \min_{w \in BV(\Omega) \cap L^2(\Omega)} \int_{\Omega} |Dw| + \frac{\lambda}{2} \int_{\Omega} (w - (g - h))^2 d\mathbf{x} + \chi_S(w + h),$$

which is equivalent to

$$(2.15) \quad \min_{w \in \Lambda - h} \left\{ E(w) := \int_{\Omega} |Dw| + \frac{\lambda}{2} \int_{\Omega} (w - (g - h))^2 d\mathbf{x} \right\},$$

where $w \in \Lambda - h$ means that $w + h \in \Lambda$. We first show that there exists a minimizer to problem (2.15). Note that w , g , and h are all in $L^2(\Omega)$, so there exists $w \in \Lambda - h$ (e.g., $w \equiv 0$) such that $E(w) < \infty$. In addition, we have $E(w) \geq 0$ for all $w \in \Lambda - h$. These properties ensure that $-\infty < \inf_{w \in \Lambda - h} E(w) < \infty$. Therefore, we can assume a minimizing sequence $\{w_n\}_{n=1}^{\infty} \subset \Lambda - h$ for problem (2.15) with $\lim_{n \rightarrow \infty} E(w_n) = \inf_{w \in \Lambda - h} E(w)$. Following the property of the minimizing sequence stated above, there exists a constant $K_1 > 0$ such that $E(w_n) \leq K_1$, namely,

$$(2.16) \quad \int_{\Omega} |Dw_n| + \frac{\lambda}{2} \int_{\Omega} (w_n - (g - h))^2 d\mathbf{x} \leq K_1,$$

which implies

$$(2.17) \quad \int_{\Omega} |Dw_n| \leq K_1.$$

Furthermore, using $0 \leq w_n(\mathbf{x}) + h(\mathbf{x}) \leq 255$ a.e. in Ω and the inclusion $W^{1,2}(\Omega) \subset W^{1,1}(\Omega) \subset L^1(\Omega)$, there exists a constant $K_2 > 0$ such that

$$(2.18) \quad \int_{\Omega} |w_n| d\mathbf{x} \leq 255|\Omega| + \int_{\Omega} |h| d\mathbf{x} \leq K_2 \quad \forall n \geq 1,$$

i.e., $\|w_n\|_{L^1(\Omega)} \leq K_2$ for all $n \geq 1$. Now, from (2.17) and (2.18) we obtain that $\{w_n\}_{n=1}^{\infty}$ is uniformly bounded in $BV(\Omega)$, i.e., $\sup \|w_n\|_{BV(\Omega)} < \infty$. By Lemma 2.5, we can deduce that there exist a subsequence $\{w_{n_k}\}_{k=1}^{\infty}$ of $\{w_n\}_{n=1}^{\infty}$ and a function $w_* \in BV(\Omega)$ such that $w_{n_k} \rightarrow w_*$ in $L^1(\Omega)$. Thus, $w_{n_k} \rightarrow w_*$ a.e. in Ω and then the Lebesgue dominated convergence theorem asserts that

$$(2.19) \quad \int_{\Omega} (w_* - (g - h))^2 d\mathbf{x} = \lim_{k \rightarrow \infty} \int_{\Omega} (w_{n_k} - (g - h))^2 d\mathbf{x}.$$

On the other hand, applying Lemma 2.6, we obtain

$$(2.20) \quad \int_{\Omega} |Dw_*| \leq \liminf_{k \rightarrow \infty} \int_{\Omega} |Dw_{n_k}|.$$

Combining (2.19) with (2.20), we have

$$(2.21) \quad E(w_*) \leq \liminf_{k \rightarrow \infty} E(w_{n_k}) = \inf_{w \in \Lambda - h} E(w).$$

Since $0 \leq w_{n_k}(\mathbf{x}) + h(\mathbf{x}) \leq 255$ a.e. in Ω , by taking the limit we have $0 \leq w_*(\mathbf{x}) + h(\mathbf{x}) \leq 255$ a.e. in Ω , which concludes that $w_* \in \Lambda - h$ is a minimizer of problem (2.15). Since the total variation defined in Definition 2.4 is convex and the L^2 data term is strictly convex, the sum of these two terms is also strictly convex. The uniqueness of the minimizer follows directly from the strict convexity of the energy functional E given in (2.15) (cf. the proof of Lemma 3.1 in [15]). Finally, note that the unique minimizer for problem (2.3) should be $u_* := w_* + h$. This completes the proof. \blacksquare

To conclude this subsection, we remark that the other case, $q = 2$, for the variational minimization problems (2.3) and (2.11) can be done in a similar way in the function space $W^{1,2}(\Omega)$.

3. The alternating minimization algorithm. Advantageously, the newly proposed models (2.3) and (2.11) can be solved very efficiently by the popular split Bregman method [11, 23]. In this subsection, we will derive the numerical algorithm for solving (2.3) in detail, and the algorithm for (2.11) is almost the same.

Without loss of generality, we first discretize the image domain as a regular Cartesian grid of size $N \times N$, i.e., $\Omega = \{(i, j) : i = 1, 2, \dots, N, j = 1, 2, \dots, N\}$, where (i, j) denotes a pixel of the image. Then grayscale images are considered as $N \times N$ matrices. Introducing the discrete gradient operator as $(\nabla u)_{i,j} = ((\nabla_x^+ u)_{i,j}, (\nabla_y^+ u)_{i,j})$ with

$$\begin{aligned} (\nabla_x^+ u)_{i,j} &:= \begin{cases} u_{i,j+1} - u_{i,j}, & 1 \leq j \leq N-1, \\ 0, & j = N, \end{cases} \\ (\nabla_y^+ u)_{i,j} &:= \begin{cases} u_{i+1,j} - u_{i,j}, & 1 \leq i \leq N-1, \\ 0, & i = N, \end{cases} \end{aligned}$$

the model (2.3) can be discretized as

$$(3.1) \quad \min_u \sum_{i,j} \left(\frac{1}{q} |(\nabla u)_{i,j} - (\nabla h)_{i,j}|^q + \frac{\lambda}{2} (u_{i,j} - g_{i,j})^2 \right) + \chi_S(u).$$

Applying the operator splitting technique [23] to (3.1), we obtain the following equivalent minimization problem:

$$(3.2) \quad \min_{u,d,v} \sum_{i,j} \left(\frac{1}{q} |d_{i,j}|^q + \frac{\lambda}{2} (u_{i,j} - g_{i,j})^2 \right) + \chi_S(v), \quad \text{subject to } d = \nabla u - \nabla h \text{ and } v = u.$$

The splitting problem (3.2) can be solved by using the Bregman iteration. Introducing two penalty parameters, $\gamma > 0$ and $\delta > 0$, we arrive at the following unconstrained minimization problem:

$$(3.3) \quad \min_{u,d,v} \sum_{i,j} \left(\frac{1}{q} |d_{i,j}|^q + \frac{\lambda}{2} (u_{i,j} - g_{i,j})^2 + \frac{\gamma}{2} |d_{i,j} - (\nabla u)_{i,j} + (\nabla h)_{i,j} - b_{i,j}|^2 + \frac{\delta}{2} (v_{i,j} - u_{i,j} - c_{i,j})^2 \right) + \chi_S(v),$$

where b and c are variables related to the Bregman iteration algorithm. Furthermore, (3.3) can be solved by alternating the search directions of u , d , and v as follows:

• **u -subproblem:**

$$(3.4) \quad u^{n+1} = \arg \min_u \sum_{i,j} \left(\frac{\lambda}{2} (u_{i,j} - g_{i,j})^2 + \frac{\gamma}{2} |d_{i,j}^n - (\nabla u)_{i,j} + (\nabla h)_{i,j} - b_{i,j}^n|^2 + \frac{\delta}{2} (v_{i,j}^n - u_{i,j} - c_{i,j}^n)^2 \right);$$

• **d -subproblem:**

$$(3.5) \quad d^{n+1} = \arg \min_d \sum_{i,j} \left(\frac{1}{q} |d_{i,j}|^q + \frac{\gamma}{2} |d_{i,j} - (\nabla u^{n+1})_{i,j} + (\nabla h)_{i,j} - b_{i,j}^n|^2 \right);$$

• **v -subproblem:**

$$(3.6) \quad v^{n+1} = \arg \min_v \sum_{i,j} \left(\frac{\delta}{2} (v_{i,j} - u_{i,j}^{n+1} - c_{i,j}^n)^2 \right) + \chi_S(v).$$

Note that Bregman variables b and c are updated by $b^{n+1} = b^n + \nabla u^n - \nabla h - d^{n+1}$ and $c^{n+1} = c^n + u^{n+1} - v^{n+1}$, respectively.

In what follows, we give more details about these subproblems. For the u -subproblem, differentiating the objective function given in (3.4) and then setting it to zero, we obtain the discrete screened Poisson equation:

$$(3.7) \quad (\lambda + \delta) u_{i,j}^{n+1} - \gamma (\Delta u^{n+1})_{i,j} = \lambda g_{i,j} - \gamma (\operatorname{div}(d^n + \nabla h - b^n))_{i,j} + \delta (v_{i,j}^n - c_{i,j}^n).$$

The discrete operators div and Δ are defined as follows [49]: given $p = (p^1, p^2)$ with $p^1, p^2 \in \mathbb{R}^{N \times N}$, we define

$$(\operatorname{div} p)_{i,j} := (\nabla_x^- p^1)_{i,j} + (\nabla_y^- p^2)_{i,j} := (p_{i,j}^1 - p_{i,j-1}^1) + (p_{i,j}^2 - p_{i-1,j}^2),$$

where ∇_x^- and ∇_y^- are backward difference operators with Neumann boundary conditions. The discrete Laplacian is then defined as the composite of ∇ and div as $\Delta u := \operatorname{div}(\nabla u)$. Since (3.7) produces a symmetric and diagonally dominant linear system, some iterative solvers such as the Jacobi method or Gauss–Seidel method can be employed for efficiently solving u .

For the d -subproblem, the objective function given in (3.5) is strictly convex and has the following closed-form solution:

$$(3.8) \quad d_{i,j}^{n+1} = \frac{(\nabla u^{n+1})_{i,j} - (\nabla h)_{i,j} + b_{i,j}^n}{|(\nabla u^{n+1})_{i,j} - (\nabla h)_{i,j} + b_{i,j}^n|} \times \max \left\{ |(\nabla u^{n+1})_{i,j} - (\nabla h)_{i,j} + b_{i,j}^n| - \frac{1}{\gamma}, 0 \right\} \quad \text{for } q = 1$$

and

$$(3.9) \quad d_{i,j}^{n+1} = \frac{\gamma}{1 + \gamma} \left((\nabla u^{n+1})_{i,j} - (\nabla h)_{i,j} + b_{i,j}^n \right) \quad \text{for } q = 2.$$

Finally, for the v -subproblem, (3.6) can be solved by pixelwise orthogonal projection of $u + c$ onto the predefined interval $S := [s_1, s_2]$:

$$(3.10) \quad v_{i,j} = \min \left\{ \max \{u_{i,j} + c_{i,j}, s_1\}, s_2 \right\}.$$

Note that we take $S = [s_1, s_2] := [0, 255]$ throughout this paper.

To sum up, the split Bregman algorithm is described in Algorithm 3.1.

Algorithm 3.1 Split Bregman algorithm for solving (2.3).

```

initialize  $u = h, v = h, d = 0, b = 0, c = 0$ 
while  $\|u - u_{prev}\|_2 / \|u\|_2 > tol$  do
    Solve the  $u$ -subproblem defined in (3.4) using (3.7)
    Solve the  $d$ -subproblem defined in (3.5) using (3.8) or (3.9)
    Solve the  $v$ -subproblem defined in (3.6) using (3.10)
     $b \leftarrow b + \nabla u - \nabla h - d$ 
     $c \leftarrow c + u - v$ 
end while

```

The convergence of Algorithm 3.1 can be guaranteed via the convergence of the ADMM [18], which we conclude as the following theorem.

Theorem 3.1. *For the minimization problem (3.2), let the initials u^0, d^0, v^0, b^0 , and c^0 be arbitrary, and let $\gamma, \delta > 0$. Then the sequence $\{u^n, d^n, v^n, b^n, c^n\}$ generated by Algorithm 3.1 converges to $\{u^*, d^*, v^*, b^*, c^*\}$, where (u^*, d^*, v^*) is the minimizer of problem (3.2).*

4. Numerical experiments. In this section, we will give some numerical examples to demonstrate the high performance of the proposed adaptive contrast enhancement model. For all test problems, the intensity values of images are in $S = [0, 255]$. We take the stopping tolerance $tol = 10^{-4}$ in Algorithm 3.1, set the two penalty parameters $\gamma = \delta = 5/255$, and choose the standard deviation of Gaussian kernel as 5 in (2.7) for all examples. The test images were downloaded from the following websites:

- Kodak Lossless True Color Image [19]: <http://r0k.us/graphics/kodak/>.
- Contrast Enhancement Evaluation Database CEED2016 [44]: <http://data.mendeley.com/datasets/3hfzp6vwkm/3>.
- Low Dynamic Range Test Images [30]: <http://mcl.korea.ac.kr/projects/LDR/>.
- Image Processing On Line [34]: <http://demo.ipol.im/demo/84/>.
- Image Processing On Line [37]: <http://demo.ipol.im/demo/107/>.
- Image Processing On Line [22]: <http://demo.ipol.im/demo/g.ace/>.

Throughout this section, we denote by f the original low-light image, by u_1 the solution of model (2.2) with $q = 1$, by u_2 the solution of model (2.2) with $q = 2$, by u_{1a} the solution of model (2.3) (or (2.11) for color images) with $q = 1$, and by u_{2a} the solution of model (2.3) (or (2.11) for color images) with $q = 2$, where the subscript “ a ” means “adaptive model.” In practice, the enhanced image by solving variational minimization problems like (1.1) is further processed by a simplest color balance (SCB) [32] with an $s\%$ of saturation. Usually, a small s like 0.1 can make the image more natural [34]. We also denote the postprocessed results

by u_{1s} , u_{2s} , u_{1as} , and u_{2as} , respectively, where the subscript “s” represents “saturation.” We will show the results of SCB postprocessing in Figures 11–12.

Example 4.1 (grayscale image enhancement). In this example, we first consider the synthetic image shown in Figure 2(a) to exhibit the innate characters of the minimizers obtained by solving the variational minimization problems (2.2) and (2.3) with $q = 1$ and $q = 2$. For simplicity, the contrast-level parameter β here is exceptionally set to be 1; i.e., there is no additional enhancement in structure. Conceptually, the original image f can be thought of as an image being nonuniformly illuminated with underexposure at pixels except for the left-central part on the image domain. The minimizers of (2.2) and (2.3) with $q = 1$ and $q = 2$ using this f as the input image are denoted by u_1 , u_2 , u_{1a} , and u_{2a} , respectively. The model parameters are $\lambda = 0.0005$ for both u_1 and u_{1a} and $\lambda = 0.001$ for both u_2 and u_{2a} . The enhanced results are displayed in Figure 2.

We can see from Figures 2(b) and 2(c) that although u_1 and u_2 elevate the dim area very well, the original bright area is also suppressed to gray, which is usually undesired in practice. The difference between u_1 and u_2 is that u_2 is much smoother and u_1 better preserves the original structure. Figures 2(d)–2(f) show the adaptive results of u_{1a} with brightness parameter α given as 0.8, 1.0, and 1.2, respectively. It can be observed that, unlike u_1 and u_2 , u_{1a} preserves the original bright area very well, and the dim area becomes much brighter as α increases. Similar results can be found in Figures 2(g)–2(i) for u_{2a} . The characters between u_{1a} and u_{2a} are apparent and quite similar to the characters between u_1 and u_2 just discussed above.

Now, we use the second grayscale image displayed in Figure 3(a) to further demonstrate the given statement for the innate characters of the four minimizers. The parameter settings are the same as those used in Figure 2, except that here we set $\beta = 3\alpha > 1$; i.e., the contrast-level parameter is set to be three times the brightness parameter (cf. Remark 4.2 below). We can see again, from Figures 3(b) and 3(c), that both u_1 and u_2 destroy the sky by suppressing it to gray, which is apparently undesired. Figures 3(d)–3(i) show the adaptive results of u_{1a} and u_{2a} with different brightness parameters. The preserved bright sky and the enhanced iris on the table exhibit the high performance of the newly proposed method.

In the computational aspect, both models (2.2) and (2.3) are implemented by the popular split Bregman algorithm as introduced in section 3. The iteration numbers are 1269 for u_1 , 610 for u_2 , (833, 862, 860) for u_{1a} with $\alpha = (0.8, 1.0, 1.2)$, respectively, and (415, 416, 388) for u_{2a} with $\alpha = (0.8, 1.0, 1.2)$, respectively. As a result, the adaptive model (2.3) is much more computationally efficient than its nonadaptive counterpart for both $q = 1$ and $q = 2$.

Remark 4.1. For a fair comparison of u_1 and u_2 with u_{1a} and u_{2a} , we have implemented an additional $\chi_S(u)$ term with $S = [0, 255]$ for model (2.2) in Example 4.1. In the next example, we will also add this term for model (2.2).

Remark 4.2. Note that although a larger α value makes the intensity of dim pixels brighter, it also makes them flatter. Intuitively, in this case, larger β should be taken to enhance the image structure. Empirically, we find that $\beta = 3\alpha > 1$ gives satisfactory results, and we will keep this fixed for all the remaining experiments in this paper.

Example 4.2 (color image enhancement). In this example, we study the effectiveness of our method for RGB color images. The general settings are the same as Example 4.1. The only

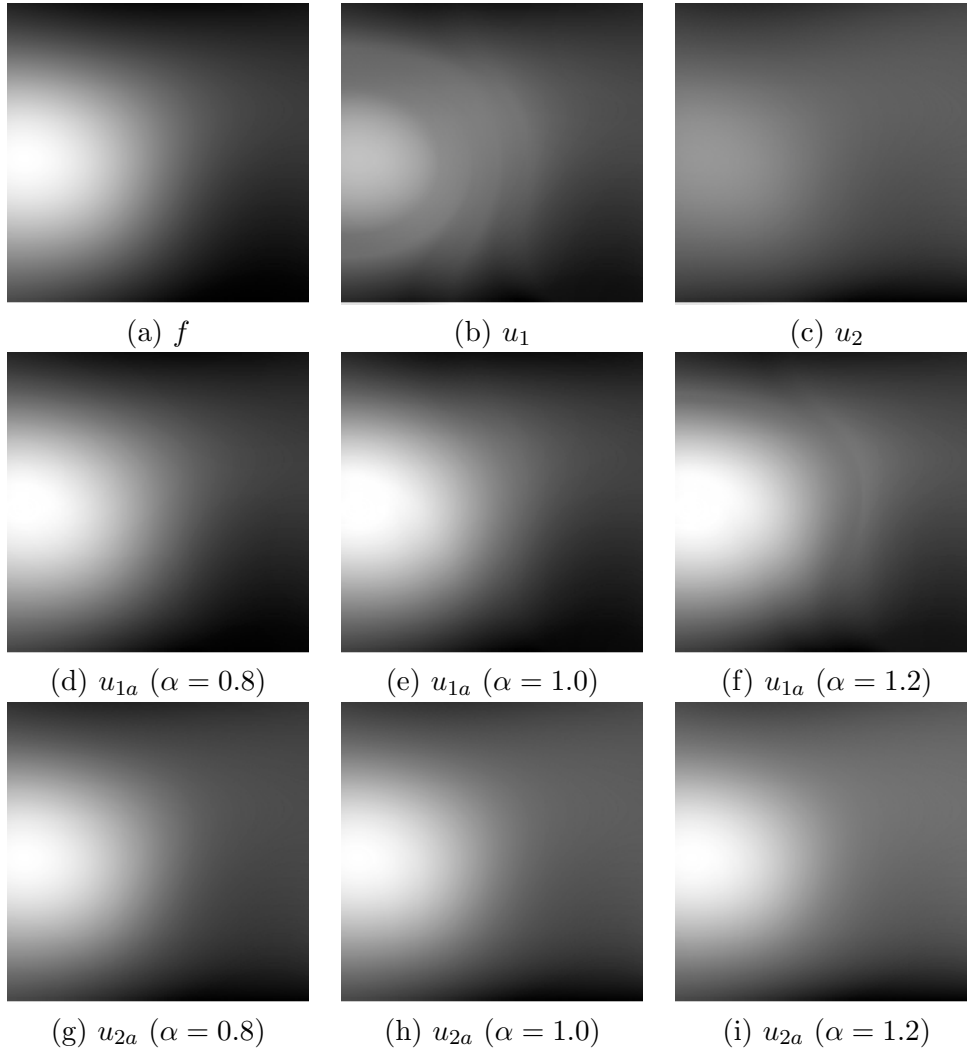


Figure 2. Numerical results of Example 4.1: (a) the original nonuniformly illuminated image; (b) the minimizer of (2.2) with $q = 1$; (c) the minimizer of (2.2) with $q = 2$; (d)–(f) the minimizer of (2.3) with $q = 1$ and various α ; (g)–(i) the minimizer of (2.3) with $q = 2$ and various α . The model parameters are $\lambda = 0.0005$ for u_1 and u_{1a} , $\lambda = 0.001$ for u_2 and u_{2a} , and $\beta = 1$ for u_{1a} and u_{2a} .

difference that should be noticed is that models (2.2) and (2.11) are employed channelwise to the RGB channels of the input color images. The first test image is shown in Figure 4(a), and the enhancement results are depicted in Figures 4(b)–4(i). Similar to the grayscale case in Figure 3, u_1 and u_2 suppress the sky to be much darker, which is undesired. On the other hand, u_{1a} and u_{2a} successfully preserve the original color in f and simultaneously recover the front of the sports car. As α gets bigger, the front becomes more discernible.

The difference between u_{1a} and u_{2a} in Figure 4 is not that significant, so we use another test image depicted in Figure 5(a) to demonstrate their difference. Comparing Figure 5(f) with

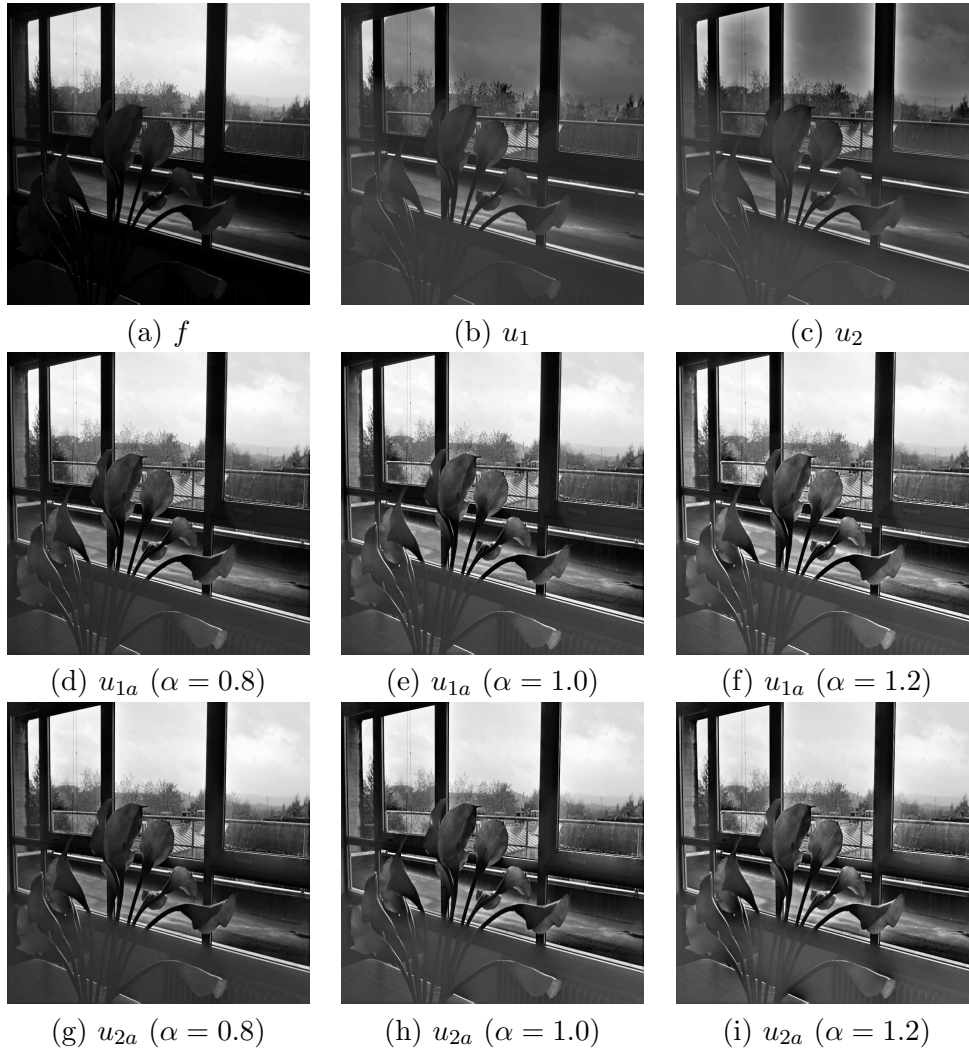


Figure 3. Numerical results of Example 4.1: (a) the original low-light image; (b) the minimizer of (2.2) with $q = 1$; (c) the minimizer of (2.2) with $q = 2$; (d)–(f) the minimizer of (2.3) with $q = 1$ and various α ; (g)–(i) the minimizer of (2.3) with $q = 2$ and various α . The model parameters are $\lambda = 0.0005$ for u_1 and u_{1a} , $\lambda = 0.001$ for u_2 and u_{2a} , and $\beta = 3\alpha > 1$ for u_{1a} and u_{2a} .

Figure 5(i), one can observe that u_{1a} has much clearer edges while u_{2a} has some blurred edges. In the computational aspect, the adaptive model (2.11) is still much more computationally efficient than its nonadaptive counterpart for both $q = 1$ and $q = 2$. For Figure 4, the average iteration numbers across RGB channels are 1161 for u_1 , 601 for u_2 , (824, 841, 859) for u_{1a} with $\alpha = (0.8, 1.0, 1.2)$, respectively, and (447, 473, 491) for u_{2a} with $\alpha = (0.8, 1.0, 1.2)$, respectively. For Figure 5, the average iteration numbers across RGB channels are 1316 for u_1 , 628 for u_2 , (955, 924, 930) for u_{1a} with $\alpha = (0.8, 1.0, 1.2)$, respectively, and (376, 394, 401) for u_{2a} with $\alpha = (0.8, 1.0, 1.2)$, respectively.

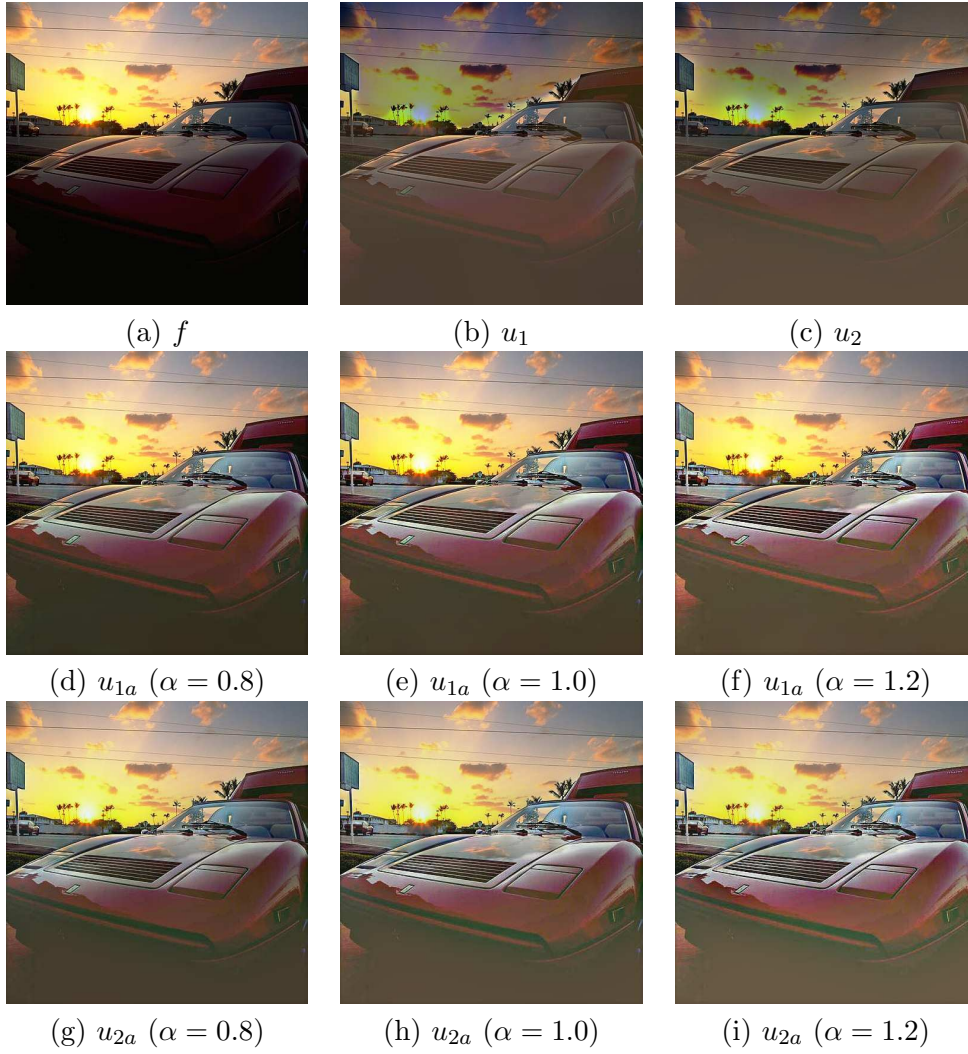


Figure 4. Numerical results of Example 4.2: (a) the original low-light image; (b) the minimizer of (2.2) with $q = 1$; (c) the minimizer of (2.2) with $q = 2$; (d)–(f) the minimizer of (2.11) with $q = 1$ and various α ; (g)–(i) the minimizer of (2.11) with $q = 2$ and various α ; the model parameters are $\lambda = 0.0005$ for u_1 and u_{1a} , $\lambda = 0.001$ for u_2 and u_{2a} , and $\beta = 3\alpha > 1$ for u_{1a} and u_{2a} .

Example 4.3 (comparison with other methods). In this example, we compare the performance of our adaptive method with the following popular enhancement methods:

- (M1) The screened Poisson equation (SPE) method [34].
- (M2) The histogram equalization (HE) method [22].
- (M3) The automatic color enhancement (ACE) method [22].
- (M4) The variational contrast enhancement (VCE) method [39].
- (M5) The contrast-limited adaptive histogram equalization (CLAHE) method [33].
- (M6) The morpho-local histogram equalization with controlled histogram equalization (MLHE-HE) method [33].

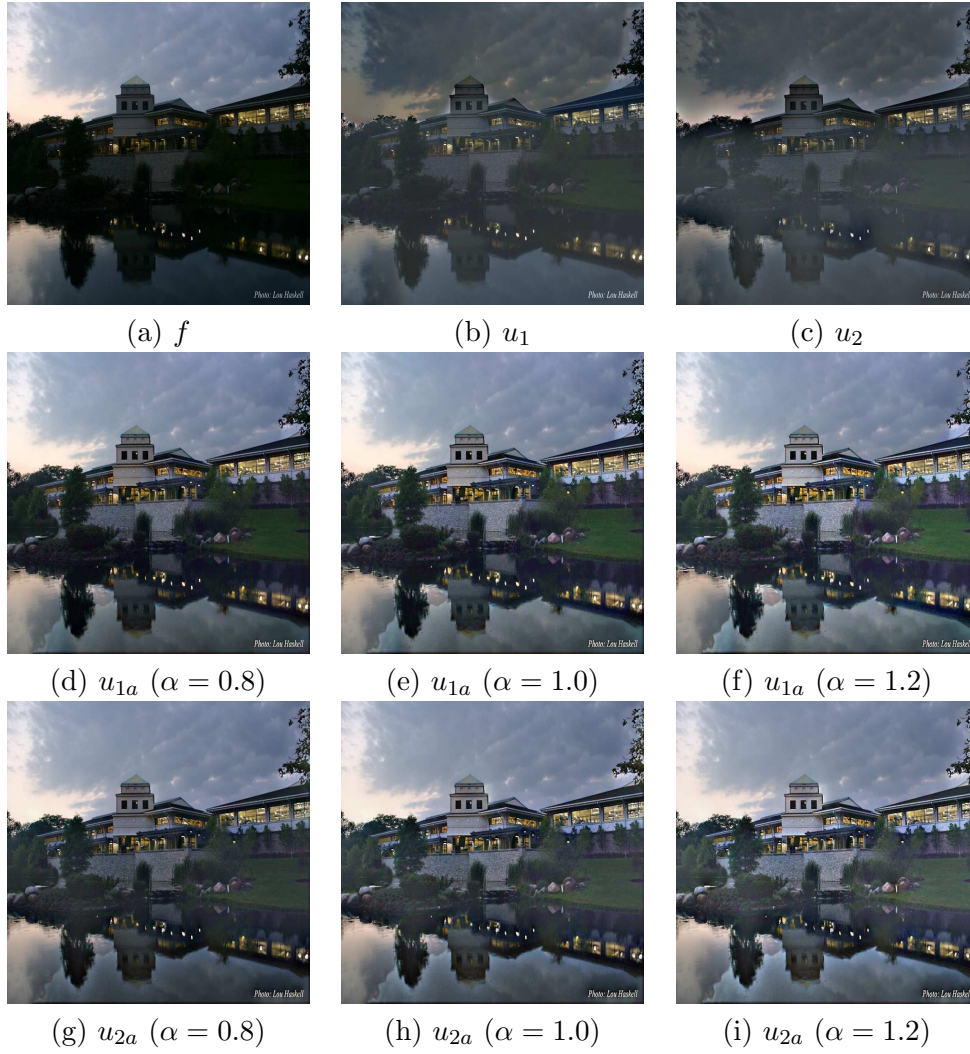


Figure 5. Numerical results of Example 4.2: (a) the original low-light image; (b) the minimizer of (2.2) with $q = 1$; (c) the minimizer of (2.2) with $q = 2$; (d)–(f) the minimizer of (2.11) with $q = 1$ and various α ; (g)–(i) the minimizer of (2.11) with $q = 2$ and various α . The model parameters are $\lambda = 0.0005$ for u_1 and u_{1a} , $\lambda = 0.001$ for u_2 and u_{2a} , and $\beta = 3\alpha > 1$ for u_{1a} and u_{2a} .

As mentioned at the beginning of this section, a saturation operation is usually performed to make images look more natural. Therefore, (M1) employs a two-stage SCB [32], each with an $s\%$ saturation operation; (M3) employs the so-called slope function [22] with a contrast-level parameter $\tilde{\alpha} \geq 1$ to perform a saturation operation; (M2) can be viewed as the limit of (M3) as $\tilde{\alpha} \rightarrow \infty$; and (M5), (M6) employ (M2) in their models. We also implement an $s\%$ SCB as a postprocessing to u_{1a} and denote the result by u_{1as} (see Figures 11 and 12). In this example, we set the saturation parameter $s = 0.1$ and the model parameter $\lambda = 0.0005$ for both (M1) and our method.

We now investigate four low-light test images, and the enhanced results of (M1)–(M6) and our method are shown in Figures 6–9. We discuss the results figure by figure. From Figures 6(b), 7(b), and 9(b), one can observe that bright sky is severely suppressed by u_{SPE} ; however, the result in Figure 8(b) is quite acceptable but still looks a little unnatural. The results by u_{HE} in Figures 6(c), 7(c), and 9(c) are very clear, but the colors do not match the original ones in f . The lower-left part in Figure 8(c) is relatively dark. For the results of u_{VCE} , the house remains dark in Figure 6(d); the scene outside the cave is enhanced, but the bricks remain unclear in Figure 7(d); the lower-left part remains dark in Figure 8(d); the mountain remains unclear in Figure 9(d). For the results of u_{CLAHE} , the sky in Figures 6(e), 7(e), and 9(e) is polluted. The lower-left part in Figure 8(e) is relatively dark. For the results of $u_{MLHE-HE}$, images are overenhanced and the hue is not preserved in Figures 6(f) and 7(f). The lower-left part in Figure 8(f) is relatively dark. The color of the tree on the left side mixes with the color of the sky in Figure 9(f). The results of u_{ACE} with various α in Figures 6(g)–6(i) look much better than the results of u_{HE} , but the colors have the same problem of not being close to the original. The results in Figures 7(g)–7(i) are acceptable, but the mountain becomes too light and unclear as α gets bigger. The results in Figures 8(g)–8(i) are also relatively dark in the lower-left parts. The sky in Figures 9(g)–9(i) looks gray.

On the other hand, the results of our method by u_{1a} perform very satisfactorily. More specifically, the colors are preserved as close as possible to f , and the house is bright in Figures 6(j)–6(l); the mountain does not fade out as α gets bigger, and the bricks are clear in Figures 7(j)–7(l); the lower-left part is relatively clear in Figures 8(j)–8(l); the sky does not turn gray and the cliff is conspicuous in Figures 9(j)–9(l). We further give a zoomed-in observation of the red rectangle on Figure 9(a) to demonstrate that our method not only elevates the intensities of dim pixels but also enhances their structures at the same time. The results are shown in Figure 10. Overall, our method is excellent in preserving the original color presented in f and boosting its dim pixels simultaneously.

Finally, we close this section by applying the newly proposed adaptive enhancement method to several low-light color images. The enhancement results of u_{1a} and u_{1as} shown in Figures 11 and 12 are satisfactory, and these show the high potential of the newly proposed model.

5. Summary and conclusions. In this paper, we have proposed a simple and efficient adaptive variational model for image contrast enhancement. This model is designed for enhancing low-light images by employing the maximum image of the RGB channels as a classifier to divide the image domain into bright and dim parts. The existence and uniqueness of minimizers for the variational minimization problem is given, and the convergent split Bregman algorithm is also provided. Numerical results obtained in this paper show the high performance of the proposed method. The most distinguished feature of the adaptive variational model is that the bright pixels are preserved as close as possible to the original ones, while the dim pixels are boosted with brightness and contrast-level parameters to adjust the degree of the strength. Extending the idea used in the proposed adaptive variational model for other types of enhancement problems such as dehazing [20] and color correction [5] should be interesting, and this deserves further study.



Figure 6. Numerical results of Example 4.3: (a) the original low-light image; (b) the enhanced result of SPE [34]; (c) the enhanced result of HE [22]; (d) the enhanced result of VCE [39]; (e) the enhanced result of CLAHE [33]; (f) the enhanced result of MLHE-HE [33]; (g)–(i) the enhanced results of ACE [22] with various α ; (j)–(l) the enhanced results of our method with $q = 1$ and various α . The model parameter $\lambda = 0.0005$ is used for both u_{SPE} and u_{1a} .



Figure 7. Numerical results of Example 4.3: (a) the original low-light image; (b) the enhanced result of SPE [34]; (c) the enhanced result of HE [22]; (d) the enhanced result of VCE [39]; (e) the enhanced result of CLAHE [33]; (f) the enhanced result of MLHE-HE [33]; (g)–(i) the enhanced results of ACE [22] with various α ; (j)–(l) the enhanced results of our method with $q = 1$ and various α . The model parameter $\lambda = 0.0005$ is used for both u_{SPE} and $u_{1\alpha}$.



Figure 8. Numerical results of Example 4.3: (a) the original low-light image; (b) the enhanced result of SPE [34]; (c) the enhanced result of HE [22]; (d) the enhanced result of VCE [39]; (e) the enhanced result of CLAHE [33]; (f) the enhanced result of MLHE-HE [33]; (g)–(i) the enhanced results of ACE [22] with various α ; (j)–(l) the enhanced results of our method with $q = 1$ and various α . The model parameter $\lambda = 0.0005$ is used for both u_{SPE} and u_{1a} .

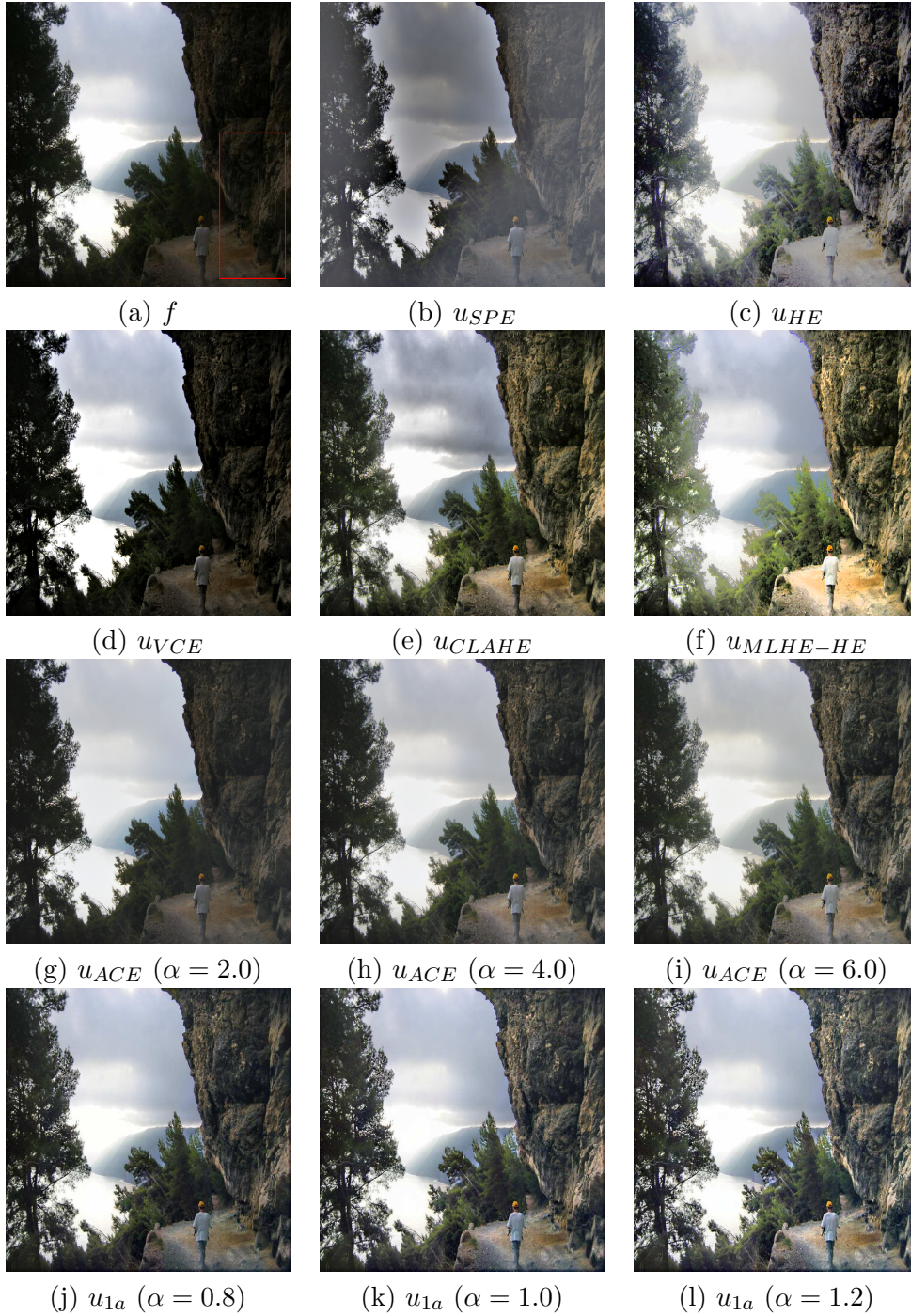


Figure 9. Numerical results of Example 4.3: (a) the original low-light image; (b) the enhanced result of SPE [34]; (c) the enhanced result of HE [22]; (d) the enhanced result of VCE [39]; (e) the enhanced result of CLAHE [33]; (f) the enhanced result of MLHE-HE [33]; (g)–(i) the enhanced results of ACE [22] with various α ; (j)–(l) the enhanced results of our method with $q = 1$ and various α . The model parameter $\lambda = 0.0005$ is used for both u_{SPE} and u_{1a} .

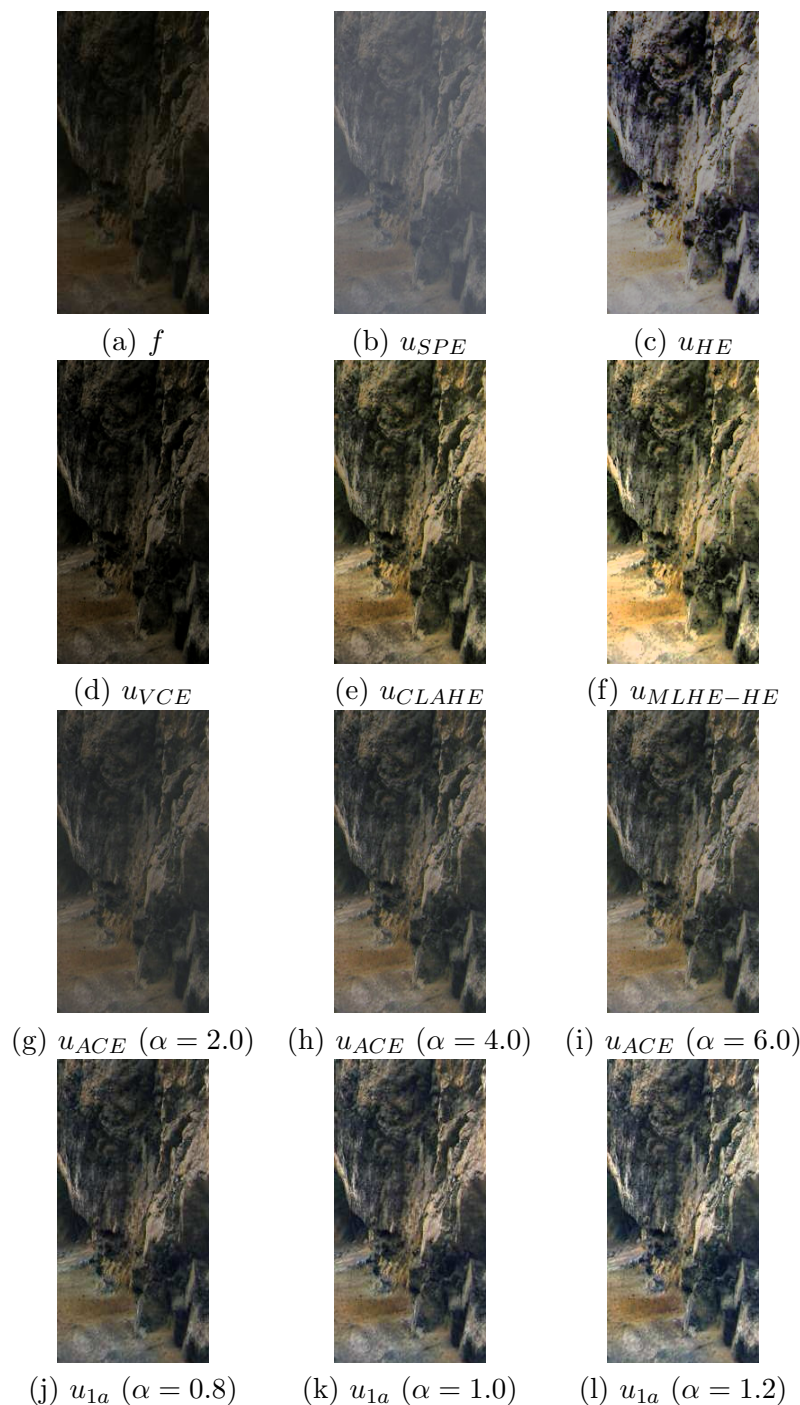


Figure 10. The locally zoomed-in results on the lower-right red rectangle of Figure 8(a): (a) the original low-light image; (b) the enhanced result of SPE [34]; (c) the enhanced result of HE [22]; (d) the enhanced result of VCE [39]; (e) the enhanced result of CLAHE [33]; (f) the enhanced result of MLHE-HE [33]; (g)–(i) the enhanced results of ACE [22] with various α ; (j)–(l) the enhanced results of our method with $q = 1$ and various α . The model parameter $\lambda = 0.0005$ is used for both u_{SPE} and u_{1a} .

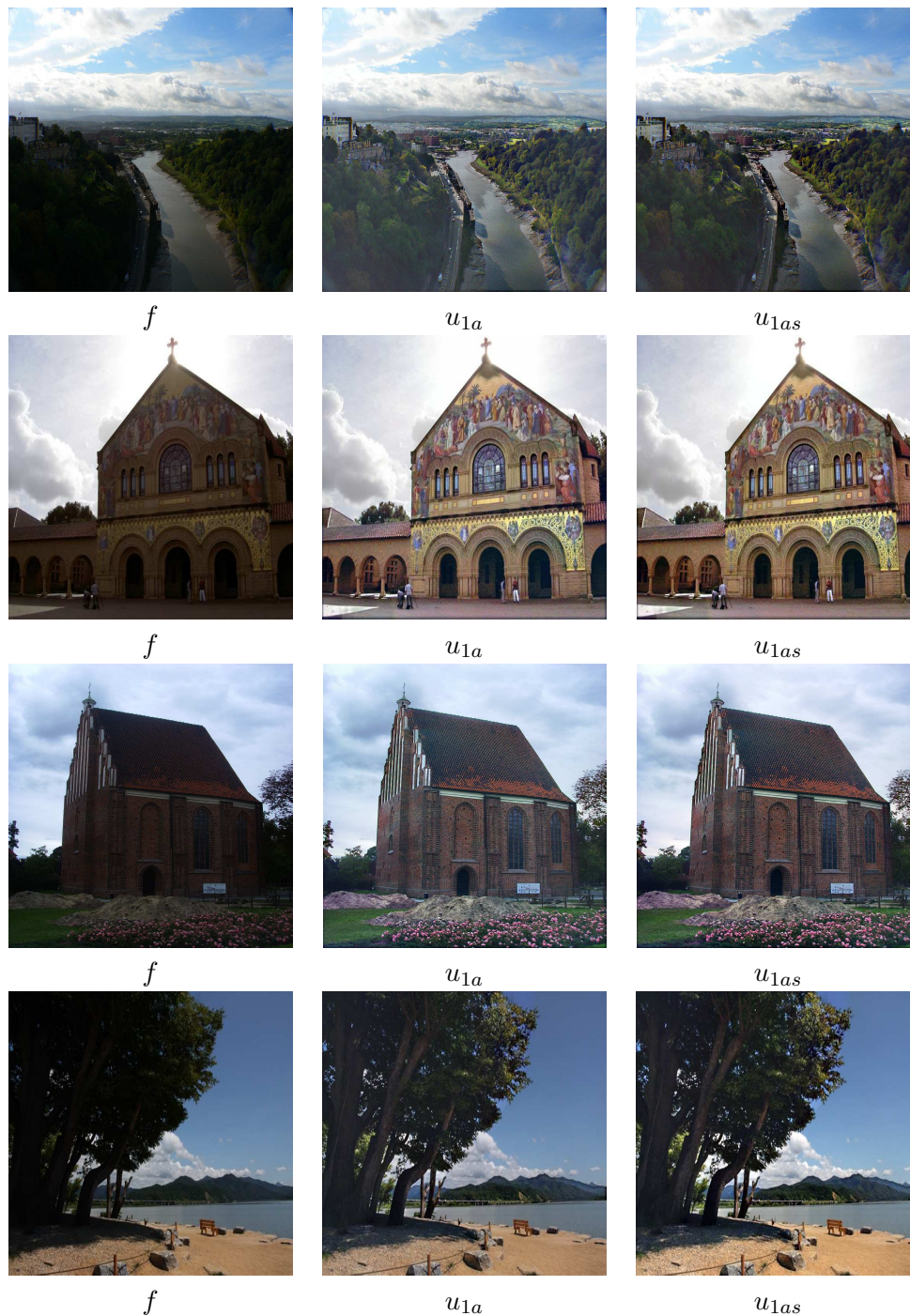


Figure 11. The enhancement results of u_{1a} and u_{1as} for several low-light color images.



Figure 12. The enhancement results of u_{1a} and u_{1as} for several low-light color images.

Acknowledgment. The authors would like to thank the three anonymous referees for their valuable comments and suggestions that led to a substantial improvement of the original manuscript.

REFERENCES

- [1] M. ABDULLAH-AL-WADUD, M. H. KABIR, M. A. A. DEWAN, AND O. CHAE, *A dynamic histogram equalization for image contrast enhancement*, IEEE Trans. Consumer Electron., 53 (2007), pp. 593–600.
- [2] L. AMBROSIO, N. FUSCO, AND D. PALLARA, *Functions of Bounded Variation and Free Discontinuity Problems*, Oxford University Press, Oxford, UK, 2000.
- [3] T. ARICI, S. DIKBAS, AND Y. ALTUNBASAK, *A histogram modification framework and its application for image contrast enhancement*, IEEE Trans. Image Process., 18 (2009), pp. 1921–1935.
- [4] S. G. BARDEJI, I. N. FIGUEIREDO, AND E. SOUSA, *Image contrast enhancement using split Bregman method*, in Proceedings of the 5th ECCOMAS Thematic Conference on Computational Vision and Medical Image Processing, 2015, pp. 63–67.
- [5] T. BATARD AND M. BERTALMÍO, *A geometric model of brightness perception and its application to color images correction*, J. Math. Imaging Vision, 60 (2018), pp. 849–881.
- [6] A. BEGHDAI AND A. L. NEGRATE, *Contrast enhancement technique based on local detection of edges*, Comput. Vision Graphics Image Process., 46 (1989), pp. 162–174.
- [7] M. BERTALMÍO, V. CASELLES, AND E. PROVENZI, *Issues about retinex theory and contrast enhancement*, Internat. J. Comput. Vision, 83 (2009), pp. 101–119.
- [8] M. BERTALMÍO, V. CASELLES, E. PROVENZI, AND A. RIZZI, *Perceptual color correction through variational techniques*, IEEE Trans. Image Process., 16 (2007), pp. 1058–1072.
- [9] G. BOCCIGNONE AND A. PICARIELLO, *Multiscale contrast enhancement of medical images*, in 1997 IEEE International Conference on Acoustics, Speech, and Signal Processing, Vol. 4, IEEE, 1997, pp. 2789–2792.
- [10] X. BRESSON AND T. F. CHAN, *Fast dual minimization of the vectorial total variation norm and application to color image processing*, Inverse Probl. Imaging, 2 (2008), pp. 455–484.
- [11] J.-F. CAI, S. OSHER, AND Z. SHEN, *Split Bregman methods and frame based image restoration*, Multiscale Model. Simul., 8 (2009), pp. 337–369, <https://doi.org/10.1137/090753504>.
- [12] V. CASELLES, J. L. LISANI, J. M. MOREL, AND G. SAPIRO, *Shape preserving local histogram modification*, IEEE Trans. Image Process., 8 (1999), pp. 220–230.
- [13] Z. CHEN, B. R. ABIDI, D. L. PAGE, AND M. A. ABIDI, *Gray-level grouping (GLG): An automatic method for optimized image contrast enhancement—part I: The basic method*, IEEE Trans. Image Process., 15 (2006), pp. 2290–2302.
- [14] S. D. CHEN AND A. R. RAMLI, *Minimum mean brightness error bi-histogram equalization in contrast enhancement*, IEEE Trans. Consumer Electron., 49 (2003), pp. 1310–1319.
- [15] Y. CHEN AND T. WUNDERLI, *Adaptive total variation for image restoration in BV space*, J. Math. Anal. Appl., 272 (2002), pp. 117–137.
- [16] H. D. CHENG AND H. XU, *A novel fuzzy logic approach to contrast enhancement*, Pattern Recognition, 33 (2000), pp. 809–819.
- [17] T. M. COVER AND J. A. THOMAS, *Elements of Information Theory*, 2nd ed., John Wiley & Sons, New York, 2006.
- [18] J. ECKSTEIN AND D. BERTSEKAS, *On the Douglas-Rachford splitting method and the proximal point algorithm for maximal monotone operators*, Math. Programming, 55 (1992), pp. 293–318.
- [19] R. FRANZEN, *Kodak Lossless True Color Image Suite*, <http://r0k.us/graphics/kodak>, 1999.
- [20] A. GALDRAN, J. VAZQUEZ-CORRAL, D. PARDO, AND M. BERTALMÍO, *Enhanced variational image de-hazing*, SIAM J. Imaging Sci., 8 (2015), pp. 1519–1546, <https://doi.org/10.1137/15M1008889>.
- [21] C. GATTA, A. RIZZI, AND D. MARINI, *ACE: An automatic color equalization algorithm*, in Proceedings of the First European Conference on Color in Graphics, Image, and Vision (CGIV02), 2002, pp. 316–320.

- [22] P. GETREUER, *Automatic color enhancement (ACE) and its fast implementation*, Image Process. On Line, 2 (2012), pp. 266–277.
- [23] T. GOLDSTEIN AND S. OSHER, *The split Bregman method for L_1 -regularized problems*, SIAM J. Imaging Sci., 2 (2009), pp. 323–343, <https://doi.org/10.1137/080725891>.
- [24] S.-C. HUANG, F.-C. CHENG, AND Y.-S. CHIU, *Efficient contrast enhancement using adaptive gamma correction with weighting distribution*, IEEE Trans. Image Process., 22 (2013), pp. 1032–1041.
- [25] S.-C. HUANG AND C.-H. YEH, *Image contrast enhancement for preserving mean brightness without losing image features*, Engng. Appl. Artif. Intell., 26 (2013), pp. 1487–1492.
- [26] Y.-T. KIM, *Contrast enhancement using brightness preserving bi-histogram equalization*, IEEE Trans. Consumer Electron., 43 (1997), pp. 1–8.
- [27] T. K. KIM, J. K. PAIK, AND B. S. KANG, *Contrast enhancement system using spatially adaptive histogram equalization with temporal filtering*, IEEE Trans. Consumer Electron., 44 (1998), pp. 82–86.
- [28] A. LAINE, J. FAN, AND W. YANG, *Wavelets for contrast enhancement of digital mammography*, IEEE Engng. Med. Biol. Mag., 14 (1995), pp. 536–550.
- [29] E. H. LAND AND J. J. MCCANN, *Lightness and retinex theory*, J. Opt. Soc. Amer., 61 (1971), pp. 1–11.
- [30] C. LEE, C. LEE, AND C.-S. KIM, *Contrast enhancement based on layered difference representation of 2D histograms*, IEEE Trans. Image Process., 22 (2013), pp. 5372–5384.
- [31] F. LI AND T. ZENG, *Variational image fusion with first and second-order gradient information*, J. Comput. Math., 34 (2016), pp. 200–222.
- [32] N. LIMARE, J.-L. LISANI, J.-M. MOREL, A. B. PETRO, AND C. SBERT, *Simplest color balance*, Image Process. On Line, 1 (2011), pp. 297–315.
- [33] J.-L. LISANI, *An analysis and implementation of the shape preserving local histogram modification algorithm*, Image Process. On Line, 8 (2018), pp. 408–434.
- [34] J.-M. MOREL, A. B. PETRO, AND C. SBERT, *Screened Poisson equation for image contrast enhancement*, Image Process. On Line, 4 (2014), pp. 16–29.
- [35] R. PALMA-AMESTOY, E. PROVENZI, M. BERTALMÍO, AND V. CASELLES, *A perceptually inspired variational framework for color enhancement*, IEEE Trans. Pattern Anal. Mach. Intell., 31 (2009), pp. 458–474.
- [36] P. PERONA AND J. MALIK, *Scale-space and edge detection using anisotropic diffusion*, IEEE Trans. Pattern Anal. Mach. Intell., 12 (1990), pp. 629–639.
- [37] A. B. PETRO, C. SBERT, AND J.-M. MOREL, *Multiscale retinex*, Image Process. On Line, 4 (2014), pp. 71–88.
- [38] A. B. PETRO, C. SBERT, AND J.-M. MOREL, *Automatic correction of image intensity non-uniformity by the simplest total variation model*, Methods Appl. Anal., 21 (2014), pp. 91–104.
- [39] F. PIERRE, J.-F. AUJOL, A. BUGEAU, G. STEIDL, AND V.-T. TA, *Variational contrast enhancement of gray-scale and RGB images*, J. Math. Imaging Vision, 57 (2017), pp. 99–116.
- [40] S. M. PIZER, E. P. AMBURN, J. D. AUSTIN, R. CROMARTIE, A. GESELOWITZ, T. GREER, AND K. ZUIDERVELD, *Adaptive histogram equalization and its variations*, Comput. Vision Graphics Image Process., 39 (1987), pp. 355–368.
- [41] A. POLESEL, G. RAMPONI, AND V. J. MATHEWS, *Image enhancement via adaptive unsharp masking*, IEEE Trans. Image Process., 9 (2000), pp. 505–510.
- [42] E. PROVENZI AND V. CASELLES, *A wavelet perspective on variational perceptually-inspired color enhancement*, Internat. J. Comput. Vision, 106 (2014), pp. 153–171.
- [43] E. PROVENZI, L. DE CARLI, A. RIZZI, AND D. MARINI, *Mathematical definition and analysis of the retinex algorithm*, J. Opt. Soc. Amer. A, 22 (2005), pp. 2613–2621.
- [44] M. A. QURESHI, A. BEGHDAI, AND M. DERICHE, *Towards the design of a consistent image contrast enhancement evaluation measure*, Signal Process. Image Commun., 58 (2017), pp. 212–227.
- [45] A. RIZZI, C. GATTA, AND D. MARINI, *A new algorithm for unsupervised global and local color correction*, Pattern Recognition Lett., 124 (2003) pp. 1663–1677.
- [46] A. RIZZI, C. GATTA, AND D. MARINI, *From retinex to automatic color equalization: Issues in developing a new algorithm for unsupervised color equalization*, J. Electron. Imaging, 13 (2004), pp. 75–84.
- [47] R. H. SHERRIER AND G. A. JOHNSON, *Regionally adaptive histogram equalization of the chest*, IEEE Trans. Med. Imaging, 6 (1987), pp. 1–7.
- [48] J. A. STARK, *Adaptive image contrast enhancement using generalizations of histogram equalization*, IEEE

- Trans. Image Process., 9 (2000), pp. 889–896.
- [49] C. WU AND X.-C. TAI, *Augmented Lagrangian method, dual methods, and split Bregman iteration for ROF, vectorial TV, and high order models*, SIAM J. Imaging Sci., 3 (2010), pp. 300–339, <https://doi.org/10.1137/090767558>.
- [50] Z. YU AND C. BAJAJ, *A fast and adaptive method for image contrast enhancement*, in Proceedings of 2004 International Conference on Image Processing, Vol. 2, 2004, pp. 1001–1004.
- [51] J. ZIMMERMAN, S. PIZER, E. STAAB, E. PERRY, W. MCCARTNEY, AND B. BRENTON, *Evaluation of the effectiveness of adaptive histogram equalization for contrast enhancement*, IEEE Trans. Med. Imaging, 7 (1988), pp. 304–312.